Temperature Compensation for Semiconductor Gas Sensors Based on Whale Optimization Algorithm–Least-squares Support Vector Machine

Yunde Xu,[1] Zhenzhen Cheng,[2*] Guofeng He,[2] and Chengwu Liang[2]

[1]School of Electrical and New Energy, Three Gorges University,
Daxue Road 8, Yichang, Hubei, 443002, China
[2]School of Electrical and Control Engineering, Henan University of Urban Construction,
Longxiang Avenue, Pingdingshan, Henan, 467041, China

A whale optimization algorithm–optimized least-squares support vector machine (WOA-LSSVM) temperature compensation model is proposed to compensate for the temperature drift of the output signal of semiconductor gas sensors in practical applications. The whale optimization algorithm is used to optimize the selection of the regularization parameter γ and the kernel function parameter σ^2 in the LSSVM model, and the temperature is corrected by predicting the output of the sensor through the parameter-optimized LSSVM model. Experimental results show that after the temperature compensation of a semiconductor gas sensor by the WOA-LSSVM model, the temperature coefficient of the sensor sensitivity is reduced from 4.21×10^{-3} before compensation to 2.001×10^{-5} after compensation, and the relative error is reduced from 17.68 to 0.08%. The prediction results of the WOA-LSSVM model are compared with those of the least-squares support vector machine, particle swarm optimization–least-squares support vector machine (PSO-LSSVM), and whale optimization algorithm–back-propagation neural network (WOA-BPNN) models. The WOA-LSSVM model had the highest compensation accuracy and can effectively improve the robustness of semiconductor gas sensors to temperature drift.

1. Introduction

The coal industry provides energy for power plants, chemicals, steel, transportation, and other industries. With the rapid development of China's economy, the coal industry has deeply penetrated various sectors in China. Real-time monitoring of toxic and hazardous gases in each process is required to ensure the safety of the production, processing, transportation, and use processes.[1,2] Semiconductor gas sensors have the advantages of a long service life, sensitivity to methane gas, a fast response time, and a simple driving circuit;[3–5] thus, they are widely used to

---

monitor gas concentrations in mines and industrial combustible gases.[6–8] However, in practice, the output of semiconductor gas sensors is considerably affected by the ambient temperature, which affects their detection accuracy.[9,10] Therefore, the temperature compensation of semiconductor gas sensors is required to minimize the effect of ambient temperature changes on the sensors and improve the measurement accuracy.

There are various methods of sensor temperature compensation, which can be divided into two categories: hardware compensation and software compensation.[11–13] Hardware compensation mainly involves using electronic devices and circuit structures with certain temperature characteristics to form a symmetrical circuit structure, which generates a signal of equal size and opposite polarity to eliminate the effect of temperature on the sensor and reduce its measurement error.[14] However, this approach has high design costs, low reliability, high power consumption, and other defects, making it inconducive to practical application in engineering.[15,16] Software compensation usually uses information fusion techniques to build algorithm models to eliminate the effect of temperature on the sensor, which is more accurate and easier to implement than hardware compensation methods and is more commonly used for sensor temperature correction.[17] Li *et al.*[18] addressed the problem of the serious degradation of the measurement accuracy of a six-axis force/torque sensor in extreme environments. They used a composite algorithm combining the simulated annealing algorithm (SAA) with the whale optimization algorithm (WOA) to optimize the least-squares support vector machine (LSSVM), which could effectively eliminate the interference of the temperature with the sensor output signal. Huang *et al.*[19] used an improved firefly algorithm (IFA) to optimize the initial threshold and weights of a back-propagation neural network (BPNN), and they established an IFA–BPNN temperature compensation model to correct the temperature-affected nonlinear output of a silicon micro-resonant accelerometer, effectively improving its measurement accuracy. Ruan *et al.*[20] established a DCQPSO-MKRVM temperature compensation model to correct the nonlinear drift of piezoresistive pressure sensors by using dynamic chaos quantum-behaved particle swarm optimization (DCQPSO) to optimize the optimal sparse weights of the kernel functions in a multi-kernel relevance vector machine (MKRVM), which improved the temperature stability and detection accuracy of the sensors. Li *et al.*[21] proposed a chaotic ions motion algorithm–optimized least-squares support vector machine (CIMA-LSSVM) temperature compensation model to eliminate the nonlinear interference of temperature on a silicon resistive pressure sensor, and the predicted results with those of the PSO-LSSVM model were compared to verify the superiority of the CIMA-LSSVM model.

To address the temperature drift problem of semiconductor gas sensors, in this study, we eliminated the influence of temperature on sensors by software compensation. The WOA was used to optimize the selection of the regularization parameter γ and the kernel function parameter σ^2 of the LSSVM, and a WOA-LSSVM model was established for the temperature correction of sensors. By comparing the temperature coefficient of the sensor sensitivity and the relative error before and after temperature compensation, we demonstrated that the WOA-LSSVM model could effectively minimize the influence of temperature changes on sensors and improve their measurement accuracy.

2.   Methods

2.1   Whale optimization algorithm

The WOA is a population intelligence optimization algorithm proposed by Mirjalili and Lewis in 2016.[22] It finds the optimal solution of an objective function by imitating the foraging behaviour of humpback whales in the ocean. The WOA has the advantages of few parameters, a simple structure, and high solution accuracy, and mainly includes three position-updating stages: encircling the prey, bubble net predation (trapping the prey using a spiral-shaped bubble net), and a random search.

After finding the prey, the group of whales approaches the nearest optimal whale individual through the exchange of information between the group members and begins to surround the prey. The whale encirclement prey phase is described by the following equation:

$$\begin{cases} X(t+1) = X^*(t) - A \cdot D, \\ D = \left| C \cdot X^*(t) - X(t) \right|, \end{cases} \tag{1}$$

where t is the number of the current iteration, $X^*(t)$ is the position of the optimal whale individual in the population, $X(t)$ is the position of this individual, and the vectors A and C are calculated using the following equations:

$$\begin{cases} A = 2a \cdot r_1 - a, \\ C = 2 \cdot r_2, \\ a = 2 - 2 \cdot t / t_{max}, \end{cases} \tag{2}$$

where t_{max} is the maximum number of iterations, r_1 and r_2 are random numbers in the interval [0, 1], and a is a convergence factor that decreases linearly from 2 to 0.

The humpback whales are so large that it is not easy for them to catch the more maneuverable fish. To catch more fish, the whales first trap the fish through a bubble net and then gradually surround the fish by moving upwards in a spiral before finally capturing the fish. The mathematical model is expressed as follows:

$$X(t+1) = X^*(t) + D_1 \cdot e^{bl} \cdot \cos(2\pi l), \tag{3}$$

$$D_1 = \left| X^*(t) - X(t) \right|, \tag{4}$$

where b is a constant used to adjust the shape of the spiral and l is a random number distributed in the range [−2, 1].

In the process of whale feeding using a bubble net, the upward spiral movement and encircling feeding are synchronized, and the probability of each activity is 50%. The mathematical model of whale feeding is expressed as

$$X(t+1) = \begin{cases} X^*(t) - A \cdot D, & P < 0.5 \\ X^*(t) + D_1 \cdot e^{bl} \cdot \cos(2\pi l). & P \geq 0.5 \end{cases} \tag{5}$$

The whale's feeding strategy depends on the value of $|A|$. When $|A| < 1$, the whale swims around the prey within a shrinking circle and along a spiral-shaped path simultaneously.[22] Otherwise, the whale randomly searches for prey, as expressed by the following mathematical model:

$$X(t+1) = X_{rand}(t) - A \cdot D_{rand}, \tag{6}$$

$$D_{rand} = |C \cdot X_{rand}(t) - X(t)|, \tag{7}$$

where X_{rand} denotes the position of a random whale individual.

2.2　Least-squares support vector machine

LSSVM is a machine learning algorithm proposed by Sukens.[23] It makes a higher-dimensional spatial linear regression problem equivalent to a low-dimensional spatial nonlinear regression problem by mapping feature vectors to higher-dimensional spaces and using a kernel function. Distinguishing itself from the conventional SVM algorithm, LSSVM uses the equation as a constraint and employs a different decision function to improve the convergence speed and accuracy of the algorithm, which is described as follows:

A set of n-dimensional vectors $\{(x_i, y_i), i = 1, 2, ..., n\}$ is given, where x_i denotes the input value of the ith sample, y_i denotes the output value of the ith sample, and n is the number of samples. The LSSVM maps the nonlinear vector $\Phi(x)$ to a high-dimensional space and converts it to the following linear programming problem:

$$y = \omega^T \cdot \Phi(x) + b, \tag{8}$$

where ω is the weight vector, and b is the deviation.

Considering the structural risk minimization principle, the linear regression problem is transformed into the optimization problem.

$$\begin{cases} \min J(\omega, e) = \dfrac{1}{2}\omega^T \omega + \dfrac{1}{2}\gamma \sum_{i=1}^{n} e_i^2, \\ y_i = \omega\ \Phi(x) + b + e_i, \end{cases} \tag{9}$$

where γ denotes the regularization parameter, and e_i denotes the error. Since ω belongs to the high-dimensional space, it cannot be solved directly and requires the introduction of the kernel function.

$$y = \sum_{i=1}^{n} a_i K(x, x_i) + b \,, \tag{10}$$

where a_i is the Lagrange multiplier and $K(x, x_i) = \exp\left(-\|x - x_i\| / 2\sigma^2\right)$ is the radial basis function (RBF) kernel function.

2.3 WOA-LSSVM model

The selection of γ and σ^2 affects the prediction results of the LSSVM model, and the traditional method of selecting these two parameters is empirical, which makes it difficult to determine the optimal γ and σ^2 and also makes the model easily fall into local optima. However, the WOA has a strong global search ability and high convergence accuracy, and it can optimize the selection of regularization parameters and kernel function parameters to improve the prediction accuracy of the LSSVM model effectively. The steps of the WOA-LSSVM model are as follows:

(1) Set the population size, the maximum number of iterations, the number of individual dimensions of the WOA, the range of selection of γ and σ^2 of the LSSVM, and the training error of the LSSVM.

(2) Generate the initial population of whales and normalize the training samples.

(3) Import the training samples into the LSSVM model. The mean square error between the predicted value of the temperature compensation model and the calibration concentration value of the training samples is used as the fitness value, and the fitness function is expressed as

$$f = \frac{1}{n} \sum_{i=1}^{n} (y_i - \hat{y}_i)^2, \tag{11}$$

where y_i denotes the actual value of the ith group of samples, $\hat{y}_i$ denotes the predicted value of the ith group of samples, and n denotes the number of samples.

(4) Calculate the fitness value of each individual and find the optimal individual.

(5) Update the parameters a, A, and C of the WOA in turn.

(6) Update the position of each individual in the population. If $|A| \geq 1$, update the individual position according to Eq. (6). If $|A| < 1$, update the individual position according to Eq. (5).

(7) Determine whether the termination iteration condition has been satisfied. If the maximum number of iterations or the training error of the LSSVM model is reached, the iteration is stopped. The values of γ and σ^2 obtained by the WOA are input into the LSSVM model, and the test samples are imported to start the training. Otherwise, return to step (3) and continue the iteration.

3. Temperature Compensation for Semiconductor Gas Sensors

3.1 Experiments

The experimental system includes an MQ-4 semiconductor gas sensor, methane gas with 5% concentration, a YC-ZC200 dual-channel manual dynamic gas distribution instrument with an accuracy of 1.5%, and an SY-400 gas mixing chamber with an operating temperature range of 0–100 °C and an accuracy of 0.1 °C (Fig. 1).

The MQ-4 semiconductor gas sensor is a combustible gas sensor manufactured by Zhengzhou Weisheng Electronic Technology Co., Ltd. in China.[24] This sensor exhibits excellent sensitivity to methane within a broad range of concentrations, and it offers notable advantages such as a prolonged lifespan, low manufacturing cost, and simplified driving circuitry. The detection circuit is shown in Fig. 2. The voltage V_H, serving as the heating voltage for the sensor, is applied to provide the sensor with a specific operating temperature. It can be supplied by either a direct current (DC) or alternating current (AC) power source. A 5 V DC power supply is selected and connected to pins 2 and 5. The parameter V_c represents the test voltage applied to the sensor. A 5
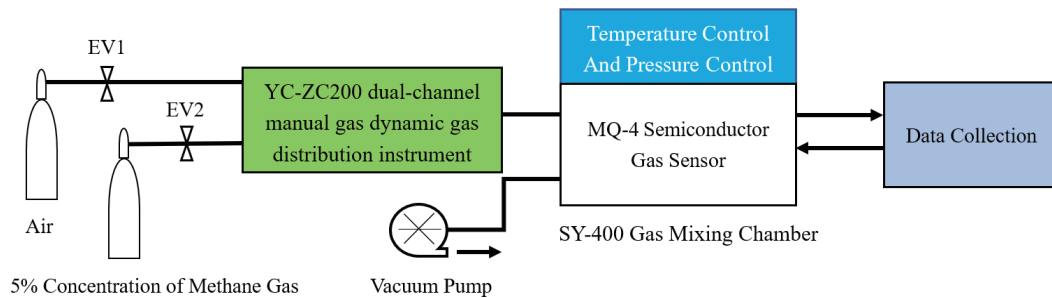
Fig. 1.   (Color online) Experimental system.
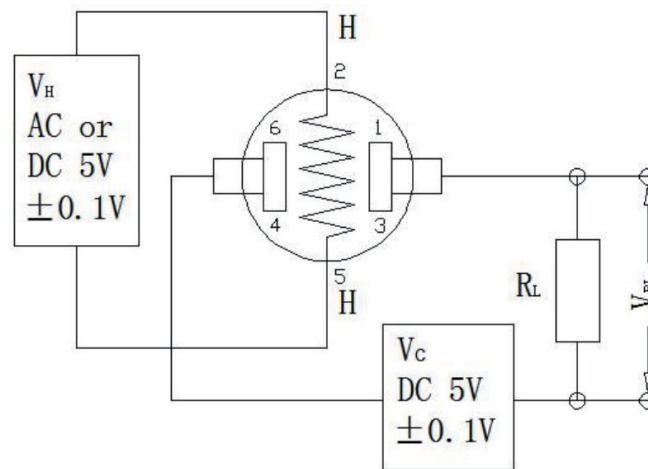
Fig. 2.   (Color online) Detection circuit.

V direct current (DC) power supply was selected to provide the test voltage to the load resistor R_L (4.7 kΩ), and V_{RL} is the voltage across the load. When the sensor detects methane gas, the resistance R_s decreases, and the output voltage V_{RL} will rise.

First, the MQ-4 semiconductor gas sensor was placed in the gas mixing chamber, the calibration temperature points were set at 9.76, 14.85, 20.87, 28.09, 36.1, 43.7, and 49.77 °C, and the humidity was maintained at 55%RH. The test gas calibration concentration range was 0–1%, and the calibration concentration point was taken every 0.1%. Then, the temperature inside the gas mixing chamber was controlled to a constant value. After the chamber was pumped into a vacuum, methane gas was introduced at the concentration of each calibration concentration point, and the sensor output voltage U_c was recorded. After all concentration points were tested, the temperature inside the gas mixing chamber was changed, and the next set of experiments was conducted.

For room temperature or low temperature (<150 °C), the adsorbed oxygen on the surface of metal oxide semiconductors is mainly in the form of O_2^-. When the sensitive material is in the heated operating state, the adsorbed O_2^- captures electrons and transforms into O^{2-} and O^-, leading to the formation of positive charges on the material's surface. This process results in a narrowing of the grain boundary barrier width and consequently leads to an increase in the conductivity and a decrease in resistance of the sensitive material. As the ambient temperature increases, the concentration of adsorbed oxygen on the surface of the sensitive material increases, and the rate of electron exchange processes accelerates,[25,26] resulting in a further decrease in the resistance of the sensitive material. Therefore, with the increase in ambient temperature, the measured output voltage of the sensor gradually increases.

Under identical experimental conditions, the experiment was repeated five times, and the average value of these five replicates was considered the outcome. The results of five experiments conducted at an ambient temperature of 20.87 °C are shown in Fig. 4. The average values of the responses at each concentration point from the five experiments are considered the final results (Fig. 3). The same approach is employed for other temperature points, indicating
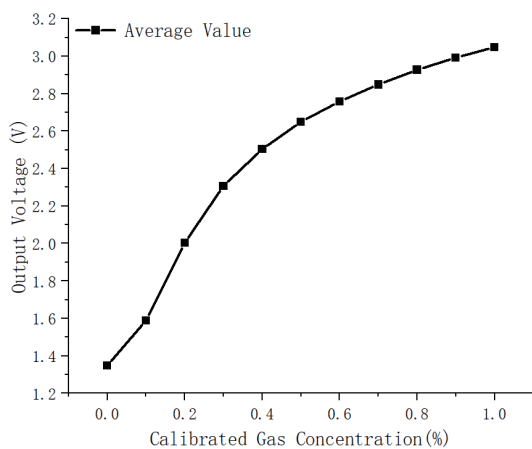
Fig. 3.   The average value of the five measurements conducted at a temperature of 20.87 °C.
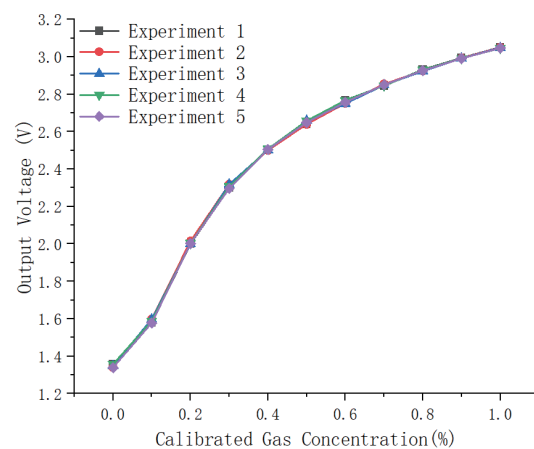
Fig. 4.   (Color online) Responses obtained from five measurements conducted at a temperature of 20.87 °C.

that the sensor has good reproducibility in response to gas concentration and temperature. The output voltage of the gas sensor underwent a nonlinear drift when the ambient temperature changed (Fig. 5), and it increased with the temperature at each calibration concentration point.

To measure the effect of the temperature on the semiconductor gas sensor, the sensitivity temperature coefficient *as* and the relative error δ_t were calculated as shown in Eqs. (12) and (13), respectively. Smaller values of these two indicators correspond to a smaller effect of a temperature change on the gas sensor.

$$a_s = \frac{\Delta U_m}{\Delta T \cdot U_{FS}} \tag{12}$$

$$\delta_t = \frac{\Delta U_m}{U_{t_{max}}} \times 100\% \tag{13}$$

Here, ΔU_m is the maximum voltage drift of the gas sensor output with the temperature at a certain calibration concentration point, ΔT is the range of the temperature change, U_{FS} is the output voltage range of the sensor, and $U_{t_{max}}$ is the maximum output voltage corresponding to ΔU_m for the sensor.

From the calculation, we obtained ΔT = 49.77–9.76 = 40.01 °C, U_{FS} = 1.8683 V, ΔU_m = 0.3147 V, and $U_{t_{max}}$ = 1.7798 V, giving a_s = 4.21 × 10^{-3}/°C and δ_t = 17.68%, which shows that the temperature change has a large effect on the output voltage of the gas sensor and that temperature correction is needed.
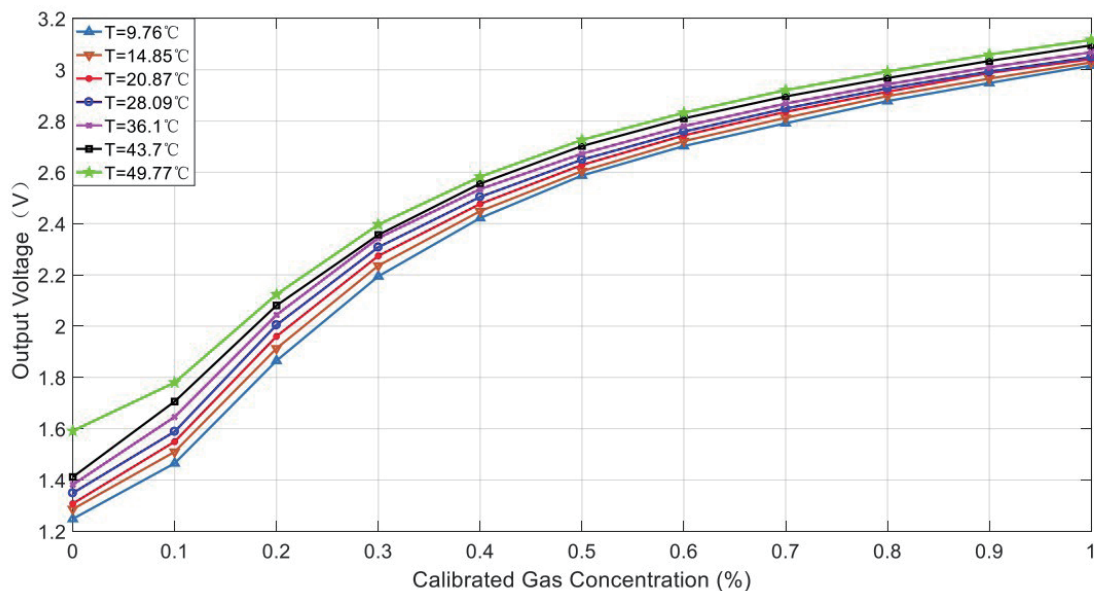
Fig. 5.   (Color online) Temperature drift characteristics of semiconductor gas sensor.

3.2   Temperature compensation

The semiconductor gas sensor was used to detect the gas concentration in the environment, its output voltage was recorded as U_c, and a temperature sensor was used to monitor the temperature in the gas mixing chamber. The output voltage of the sensor was recorded for each concentration point at each calibration temperature point. The data set consisting of the calibration temperature point and the output voltage of the gas sensor was divided into training and test samples for training the WOA-LSSVM model (Fig. 6). The output C' of the model is the predicted value of the gas concentration and is used for the temperature compensation of the gas sensor.

The parameter settings in the WOA-LSSVM model are shown in Table 1. The optimal γ obtained by optimizing the LSSVM model with the WOA is 5000, and the optimal σ^2 is 0.0334. The sensor input and output characteristic curves after temperature correction by the WOA-LSSVM model are shown in Fig. 7. It can be seen that the output of the semiconductor gas sensor was almost unaffected by the temperature after temperature correction by the WOA-LSSVM model, indicating that it can effectively improve the robustness of semiconductor gas sensors to temperature drift.

The sensitivity temperature coefficient a_s and the relative error δ_t of the semiconductor gas sensor after temperature correction were calculated as

$$a_s = \frac{\Delta C_m}{\Delta T \cdot C_{FS}},$$ (14)

$$\delta_t = \frac{\Delta C_m}{C_{t_{max}}} \times 100\%,$$ (15)
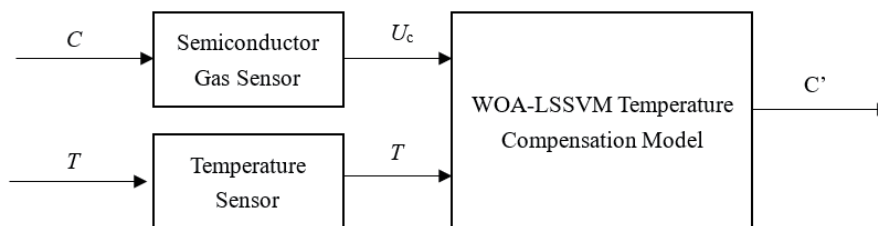
Fig. 6.   Schematic of temperature compensation.

Table 1
Parameter settings in the WOA-LSSVM model.

Model	Population size	Maximum iteration	Dimension	Search space	Training error
WOA-LSSVM	30	100	2	γ: [0.01, 5000] σ^2: [0.01, 100]	10^{-8}
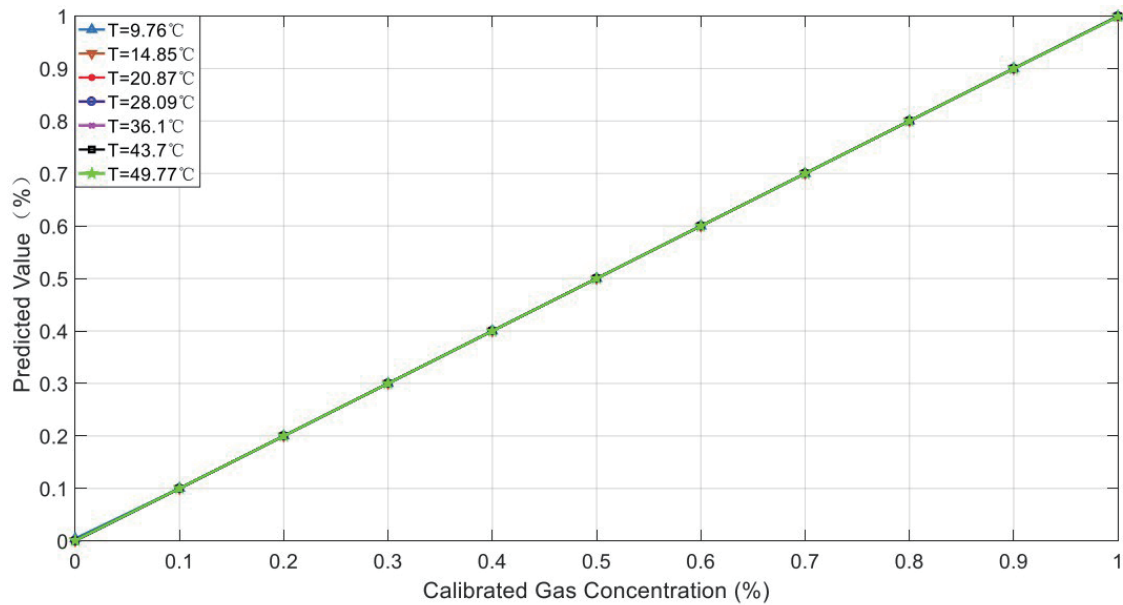
Fig. 7.   (Color online) Sensor output characteristic curve after temperature compensation.

where ΔC_m is the maximum value of the predicted concentration of the gas sensor with the temperature drift at a certain calibration concentration point, ΔT is the range of the temperature change, C_{FS} is the predicted concentration range of the sensor, and $C_{t_{max}}$ is the maximum predicted concentration value corresponding to ΔC_m.

From the calculation, we obtained $\Delta T = 49.77 - 9.76 = 40.01$ °C, $C_{FS} = 0.9994$, $\Delta C_m = 0.0008$, and $C_{t_{max}} = 0.9996$, giving $a_s = 2.001 \times 10^{-5}$/°C and $\delta_t = 0.08\%$. The values of a_s and δ_t for the semiconductor gas sensor after temperature compensation by the WOA-LSSVM model were two orders of magnitude lower than those before temperature compensation; thus, the effect of temperature on the sensor is substantially reduced (Table 2).

3.3   Comparison of different algorithm models

To verify the optimization performance of WOA-LSSVM, we also employed the LSSVM, PSO-LSSVM, and WOA-BPNN models for temperature compensation of the semiconductor gas sensor. Here, the LSSVM used the RBF as the kernel function, and γ and σ^2 were chosen as 2000 and 0.01, respectively. The parameter settings of the PSO-LSSVM and WOA-BPNN models are shown in Table 3. The PSO-LSSVM model used the RBF as the kernel function, and the optimal γ obtained by optimizing the LSSVM with the PSO algorithm was 4833.5, and the optimal σ^2 was 0.01.

The fitness curves of the algorithms are shown in Fig. 8. It can be seen that the WOA-BPNN model falls into a local optimum after 46 iterations, the PSO-LSSVM model reaches the global optimum after 73 iterations, and the WOA-LSSVM model converges to the global optimum after eight iterations. Moreover, its convergence accuracy was higher than that of the PSO-LSVVM and WOA-BPNN models.

Table 2
Comparison of results before and after temperature compensation.

Anti-temperature interference performance	Before temperature compensation	After temperature compensation with WOA-LSSVM model
a_s	4.21×10^{-3}	2.001×10^{-5}
δ_t (%)	17.68	0.08

Table 3
Parameter settings in PSO-LSSVM and WOA-BPNN models.

Model	Population size	Maximum iteration	Dimension	Search space	Training error
PSO-LSSVM	30	100	2	γ : [0.01, 5000] σ^2: [0.01, 100]	10^{-8}
WOA-BPNN	30	100	21	[−5, 5]	10^{-8}
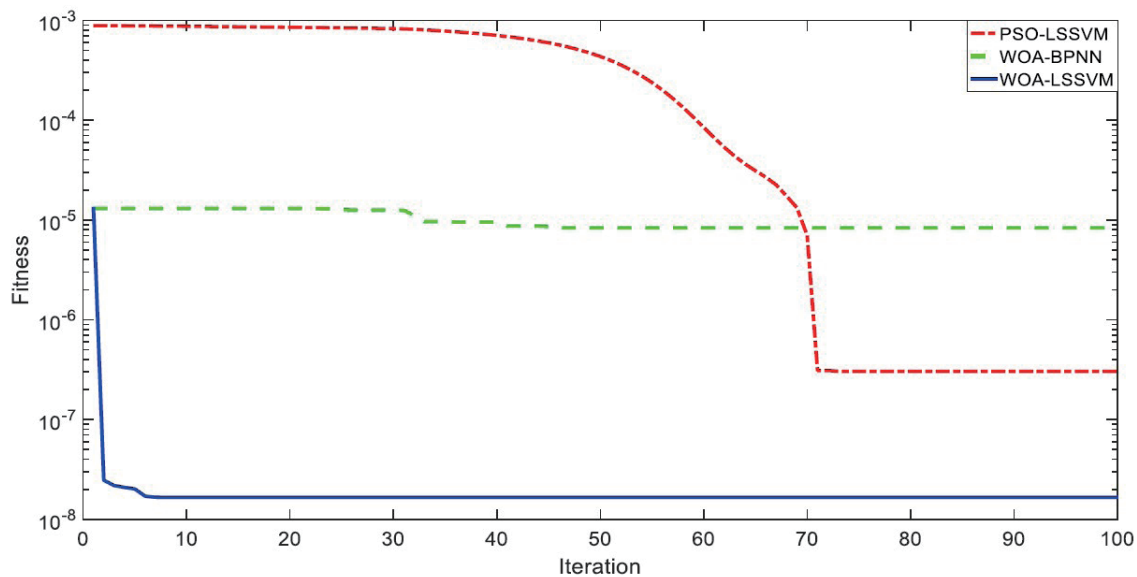
Fig. 8.   (Color online) Iteration curve of the fitness of each temperature compensation model.

The temperature coefficient of sensitivity a_s, relative error δ_t, and mean square error (*MSE*) of the semiconductor gas sensor after temperature compensation were calculated from the prediction results of the LSSVM, WOA-BPNN, PSO-LSSVM, and WOA-LSSVM models (Table 4).

It can be seen from Table 4 that after the temperature correction of the semiconductor gas sensors using the WOA-LSSVM model, a_s, δ_t, and the *MSE* between the predicted value and the calibration concentration point for the test sample were smaller than those for the LSSVM, WOA-BPNN, and PSO-LSSVM models. This indicates that the WOA-LSSVM temperature compensation model has higher compensation accuracy and better generalization performance. Using the WOA-LSSVM model for temperature compensation can effectively reduce the sensitivity drift of semiconductor gas sensors and improve their measurement accuracy.

Table 4
Comparison of performance of different algorithm models.

Performance	LSSVM	WOA-BPNN	PSO-LSSVM	WOA-LSSVM
a_s	8.262×10^{-5}	3.279×10^{-4}	6.005×10^{-5}	2.001×10^{-5}
δ_t (%)	0.33	1.33	0.24	0.08
MSE	3.8592×10^{-6}	1.4346×10^{-5}	2.2928×10^{-6}	3.5970×10^{-7}

4. Conclusions

To minimize the effect of temperature drift on the measurement accuracy of semiconductor gas sensors, we presented a WOA-LSSVM model for eliminating the nonlinear error of the sensor output. The WOA was used to select the optimal γ and σ^2 in the LSSVM, and the optimized LSSVM model was used to predict the output concentration values of the semiconductor gas sensor. We compared the results for a semiconductor gas sensor before and after temperature compensation using the WOA-LSSVM model. We found that the sensitivity temperature coefficient a_s and relative error δ_t were reduced by two orders of magnitude after temperature compensation. According to the results for temperature compensation and comparisons with other models, the WOA-LSSVM model can effectively eliminate the nonlinear effects of temperature on the sensor output, making it a feasible and competitive temperature compensation method for semiconductor gas sensors.

Acknowledgments

References

1 S. Uma and M. K. Shobana: Sens. Actuators, A **349** (2023) 114044. https://doi.org/10.1016/J.SNA.2022.114044
2 Y. Tang, Y. N. Zhao, and H. Liu: ACS Sens. **7** (2022) 3582. https://doi.org/10.1021/acssensors.2c01142
3 M. V. Nikolic, V. Milovanovic, Z. Z. Vasiljevic, and Z. Stamenkovic: Sensors **20** (2020) 6694. https://doi.org/10.3390/S20226694
4 R. A. Potyrailo: Chem. Rev. **23** (2016) 14918. https://doi.org/10.1021/acs.chemrev.6b00741
5 T.-Y. Lai, T.-H. Fang, Y.-J. Hisao, and C.-A. Chan: Vacuum **166** (2019) 155. https://doi.org/10.1016/j.vacuum.2019.04.061
6 K. G. Krishna, S. Parne, N. Pothukanuri, V. Kathirvelu, S. Gandi, and D. Joshi: Sens. Actuators, A **341** (2022) 113578. https://doi.org/10.1016/j.sna.2022.113578
7 G. Fedorenko, L. Oleksenko, N. Maksymovych, G. Skolyar, and O. Ripko: Nanoscale Res. Lett **12** (2017) 329. https://doi.org/10.1186/s11671-017-2102-0
8 Z. Y. Yuan, C. Yang, and F. L. Meng: Chemosensors **9** (2021) 179. https://doi.org/10.3390/CHEMOSENSORS9070179
9 A. Dey: Mater. Sci. Eng., B **229** (2018) 206. https://doi.org/10.1016/j.mseb.2017.12.036
10 Z. Z. Jiang, P. Xu, Y. B. Du, F. Yuan, and K. Song: Sensors **21** (2021) 3403. https://doi.org/10.3390/S21103403
11 W. Xu, X. Y. Feng, and H. Y. Xing: Electronics **8** (2019) 425. https://doi.org/10.3390/electronics8040425
12 H. X. Wang and J. Li: Sensors **22** (2022) 8309. https://doi.org/10.3390/S22218309
13 C. Liu, Z. H. Duan, B. Y. Zhang, Y. Zhao, Z. Yuan, Y. J. Zhang, Y. M. Wu, Y. D. Jiang, and H. L. Tai: Sens. Actuators, B **378** (2023) 133113. https://doi.org/10.1016/j.snb.2022.133113

14   P. R. Nagarajan, B. George, and V. J. Kumar: IEEE Sens. J. **17** (2017) 1696. https://doi.org/10.1109/jsen.2017.2653227

15   H. B. Liang, H. F. Chen, and Y. J. Lu: J. Intell. Fuzzy Syst. **37** (2019) 3113. https://doi.org/10.3233/JIFS-179114

16   S. A. Schober, Y. Bahri, C. Carbonelli, and R. Wille: Chemosensors **10** (2022) 152. https://doi.org/10.3390/CHEMOSENSORS10050152

17   N.-W. Moon and Y.-H. Kim: IEEE Sens. J. **15** (2015) 4612. https://doi.org/10.1109/JSEN.2015.2421516

18   X. H. Li, L. F. Gao, H. B. Cao, Y. X. Sun, M. Jiang, and Y. Zhang: Sensors **22** (2022) 13. https://doi.org/10.3390/S22134809

19   L. B. Huang, L. Jiang, L. Y. Zhao, and X. K. Ding: Micromachines **13** (2022) 1054. https://doi.org/10.3390/MI13071054

20   Y. Ruan, L. F. Yuan, W. B. Yuan, Y. G. He, and L. Lu: IEEE Trans. Instrum. Meas. **70** (2021) 1. https://doi.org/10.1109/TIM.2021.3089236

21   J. Li, G. Q. Hu, Y. H. Zhou, C. Zou, W. Peng, and S. M. Jahangir Alam: Sensors **16** (2016) 1707. https://doi.org/10.3390/s16101707

22   S. Mirjalili and A. Lewis: Adv. Eng. Software **95** (2016) 51. https://doi.org/10.1016/j.advengsoft.2016.01.008

23   J. A. K. Suykens and J. Vandewalle: Neural Process. Lett **9** (1999) 293. https://doi.org/10.1023/A:1018628609742

24   MQ-4: https://www.winsensor.com/product/1025.html (accessed May 2023).

25   W. J. Zhao, K. L. Ding, Y. S. Chen, F. Y. Xie, and D. Xu: IEEE Sens. J. **20** (2020) 10433. https://doi.org/10.1109/JSEN.2020.2993055

26   H. Y. Ji, Y. Liu, H. M. Zhu, H. N. Zhang, Z. Y. Yuan, and F. L. Meng: Sens. Actuators, B **388** (2023) 133874. https://doi.org/10.1016/j.snb.2023.133874

About the Authors

Yunde Xu received his B.S. degree from Xinyu University, China, in 2021. He is now studying for his M.S. degree at Three Gorges University, Yichang, China. His research interest is gas sensor temperature compensation. (1149366080@qq.com)

Zhenzhen Cheng received her M.S. degree from Taiyuan University of Technology, China, in 2009 and her Ph.D. degree from Xi'an Jiaotong University, China, in 2021. Her current research interest is ionization micro–nano intelligent sensors. (84820351@qq.com)

Guofeng He received his M.S. degree in electrical engineering from Shandong University, Shandong, China, in 2004 and his Ph.D. degree in power electronics from Zhejiang University, Hangzhou, China, in 2014. His current research interests include digital control of parallel UPS systems, high-frequency, high-power conversion, and renewable energy power conversion systems. (dragonhgf@hncj.edu.cn)

Chengwu Liang received his M.S. degree in information and communication engineering from the University of Electronic Science and Technology of China, China, and his Ph.D. degree in information and communication engineering from Zhengzhou University, China. His current research interests are interpretable artificial intelligence, including statistical machine learning, computer vision, and statistical pattern recognition, especially video understanding. (liangchengwu0615@126.com)